

# Some Analytical and Numerical Solutions to Inverse Problems Applied to Optimizing Phase-Transformation Tracking in Gas Quenching

Michael Vynnycky  
Jérôme Ferrari

FaxénLaboratoriet,  
KTH, 100 44 Stockholm, Sweden

Noam Lior  
Department of Mechanical Engineering and  
Applied Mechanics,  
University of Pennsylvania,  
Philadelphia, PA 19104-6315

*A transient inverse heat conduction problem focused on gas quenching of steel plates and rings is posed and solved, both analytically and numerically. The quenching objective is to calculate the transient convective heat transfer coefficient which would produce an optimized phase transformation cooling curve. The governing nonlinear heat equation is nondimensionalised, and a small parameter, the reciprocal of the Fourier number, is identified. This allows the construction of an analytic solution in the form of an asymptotic series. For higher values of the reciprocal Fourier number, a numerical scheme incorporating the function specification and Keller Box methods is used to generate solutions. Comparison of the results proves favorable, and suggests that for this inverse problem asymptotic methods provide an attractive alternative to solely numerical ones. [DOI: 10.1115/1.1517271]*

*Keywords:* Inverse Heat Transfer Solutions, Gas Quenching, Heat Treatment, Metal Phase Transformation, Transient Heat Conduction

## Introduction

Quenching is one of the most critical operations in the heat treatment of many metallic parts, affecting internal structure, both mechanical properties and the shape of the product. In the case of steel alloys, one desirable aim is to be able to convert austenite to martensite, while limiting the formation of pearlite and bainite, through appropriately rapid cooling of the quenched part. The cooling rate is determined by ensuring that the temperature during the cooling process never exceeds anywhere in the part the temperature which would cause transformation to undesirable phases at that location. The transformation temperatures can be found in applicable cooling-transformation phase change diagrams for the alloy in question. Practically, this leads to the prescription of a time-dependent temperature profile in the interior of the considered geometry, an objective being to find the magnitude and time dependence of the surface cooling convective heat transfer coefficient which would bring this curve about; this amounts to the formulation of an inverse heat conduction problem (IHCP). In the last decade or so, gas quenching has been gradually and increasingly developed, for environmental, quality and economical reasons to replace the traditional quenching in liquids. This process imposes new computational and fluid dynamics challenges with which FaxénLaboratoriet at the Royal Institute of Technology (KTH) has been involved for the past several years (cf. [1]). This paper presents an approach to the solution of some basic inverse heat conduction problems related to the process. Reference citations to past work related to this subject are given below in the body of the paper.

Quenched part geometries of a plate and of a ring, as in Figs. 1(a) and 1(b) respectively, with temperature-dependent thermal conductivity, are considered. Analytical and numerical approaches are adopted for the plate. Nondimensionalisation of the governing equations gives the Fourier number (Fo) as a controlling param-

eter which, if large enough (as is the case for thin enough rings or plates), permits the construction of an asymptotic series solution. An interesting feature here is that the inverse problem is reduced to an infinite sequence of direct initial value problems, analogous to the analytical solution of Burggraf [2], although obtained by a different approach. For smaller values of the Fourier number, a numerical approach is necessary and this is done through a novel application of the function specification method using future time steps, coupled with the Keller Box method for a nonlinear heat equation, a related linear sensitivity equation and a further variational equation. Good agreement with the heat transfer coefficient that would be required to achieve a desired cooling curve is obtained in the thin plate case, and the numerical scheme developed allows an estimate of the validity of the asymptotic method as the plate thickness is increased.

The equivalent problem for the ring is found, however, to have considerably more possibilities; amongst these is the fact that unequal cooling at its inner and outer surface can lead to a change in position of the maximum temperature point, and thence to a more intricate mathematical formulation for the inverse problem. Consequently, this problem is deferred to later work. For the case of a thin ring, however, asymptotic analytic progress is again possible and, under symmetrical heating conditions, the heat transfer coefficient required is found to differ from that for a thin plate only at  $O(\text{Fo}^{-3})$ .

## Formulation

Consider the cooling of a steel plate of thickness  $2L$ , initially at a uniform temperature  $T_i$ . At time  $t > 0$ , the outer surfaces of the plate at  $x = \pm L$  are subjected to cooling by means of a time-dependent heat transfer coefficient  $h(t)$ . Throughout the process, the ambient temperature  $T_\infty$  is assumed to be constant. One-dimensional heat conduction in the plate is then given by

$$\rho c_p(T) \frac{\partial T}{\partial t} = \frac{\partial}{\partial x} \left( k(T) \frac{\partial T}{\partial x} \right), \quad (1)$$

where, most generally, the specific heat capacity  $c_p$  and the

Contributed by the Heat Transfer Division for publication in the JOURNAL OF HEAT TRANSFER. Manuscript received by the Heat Transfer Division May 30, 2001; revision received August 5, 2002. Associate Editor: G. S. Dulikravich.

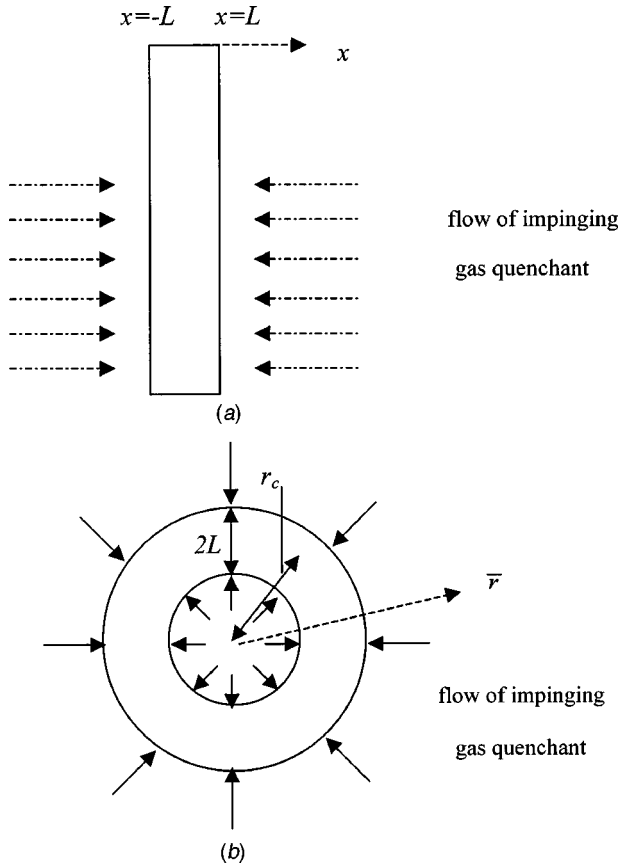


Fig. 1 Schematic of the problem for: (a) a plate; (b) a ring.

thermal conductivity  $k$  are assumed to be functions of temperature. Assuming symmetry about  $x=0$ , we have the boundary conditions

$$\frac{\partial T}{\partial x} = 0 \quad \text{at } x=0, \quad (2)$$

$$k \frac{\partial T}{\partial x} = -h(T - T_\infty) \quad \text{at } x=L, \quad (3)$$

and the initial condition

$$T = T_i \quad \text{at } t=0. \quad (4)$$

In direct problems,  $h(t)$  and  $T_\infty$ , are prescribed, enabling the straightforward determination of the temperature at any location within the plate. However, of greater interest here is the inverse problem, where a certain temperature profile (meaning a temperature-time curve) is desired at a location within the plate, and an appropriate  $h(t)$  must be found to satisfy this constraint. Typically, inverse heat conduction problems of this type have been motivated by the need to determine surface heat transfer coefficients from experimental measurements taken in the interior of a given body; consequently, the associated literature contains numerous contributions which deal with treating the effects of experimental uncertainty (see [3] for a comprehensive recent review). Here, on the other hand, the focus is on being able to cool the plate in such a way as to convert austenite to martensite, whilst limiting the formation of bainite and pearlite, all that at cooling rates which vary with the progress of the phase transformation in a way that tends to minimize distortion of the part and gas fan power consumption. At the simplest level, this involves coupling information derived from a metal phase transformation TTT-diagram (time-temperature-transformation) with the solution to the heat equation. For example, it is clear that martensite con-

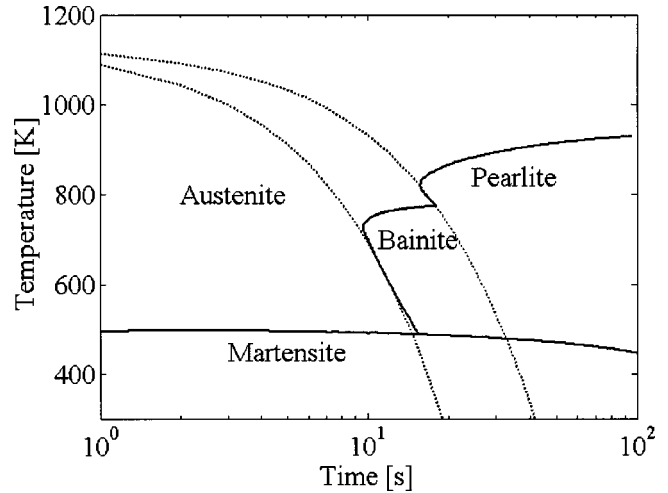


Fig. 2 CCT diagram for SAE 52100 steel

centration can be maximized simply by ensuring that the hottest point of the plate follows a cooling curve lying below the pearlite and bainite 'noses,' which can be seen in Fig. 2. In quenching practice, conventionally using liquid quenchants, the cooling rate is constant and determined by the highest temperature profile slope dictated by the transformation diagram. Since it is more difficult to attain high cooling rates when using gas as quenchant, the cooling rate can be reduced during the process to achieve just the needed one. Furthermore, it is evident that this strategy would offer a better way of controlling the final composition than, for instance, cooling at a constant rate, as is given in continuous cooling transformation (CCT) diagrams such as Fig. 2. We proceed therefore by requesting

$$T = T_w(t) \quad \text{at } x=0, \quad (5)$$

where, for  $0 \leq t \leq t_f$ , where  $t_f$  denotes the finishing time for quenching, the profile  $T_w(t)$  lies below the curves for phase transformation to bainite and pearlite; for the case of a plate, it is at once clear that, in the absence of heat evolved during phase transformation, the maximum temperature will always be found at  $x=0$ .

Nondimensionalising with

$$X = \frac{x}{L}, \quad \tau = \frac{t}{t_f}, \quad \theta = \frac{T}{T_i},$$

we have, for  $0 \leq X \leq 1$  and  $0 \leq \tau \leq 1$ ,

$$\tilde{c}_p(\theta) \frac{\partial \theta}{\partial \tau} = \text{Fo} \frac{\partial}{\partial X} \left( \tilde{k}(\theta) \frac{\partial \theta}{\partial X} \right), \quad (6)$$

where  $\tilde{k}$  and  $\tilde{c}_p$  denote, respectively, the dimensionless thermal conductivity and specific heat capacity, given by

$$\tilde{k} = \frac{k}{[k]}, \quad \tilde{c}_p = \frac{c_p}{[c_p]}.$$

Here,  $[k]$  and  $[c_p]$  denote characteristic values for these quantities, and are also used in the definition of the Fourier number, Fo, through

$$\text{Fo} = \frac{[k]t_f}{\rho[c_p]L^2}.$$

Equation (6) is then subject to the boundary conditions

$$\frac{\partial \theta}{\partial X} = 0, \quad \theta = \theta_w(\tau) \quad \text{at } X=0, \quad (7)$$

where  $\theta_w = T_w/T_i$ , and the initial condition

$$+gv=1 \quad \text{at } \tau=0. \quad (8)$$

As usual in the inverse formulation, Eq. (3) is used *a posteriori* to determine the required heat transfer coefficient, which in terms of the dimensionless variables is given by

$$h = -\frac{[k]}{L} \left[ \tilde{k}(\theta) \frac{\partial \theta}{\partial X} \right]_{X=1}, \quad (9)$$

where  $\theta_\infty = T_\infty / T_i$ .

### Asymptotic Analysis for $Fo \gg 1$ : Plates

For sufficiently large values of the Fourier number, corresponding to thin plates, an asymptotic series solution is possible. Writing

$$\theta(X, \tau) = \theta_0(X, \tau) + Fo^{-1}\theta_1(X, \tau) + Fo^{-2}\theta_2(X, \tau) + O(Fo^{-3})$$

Eq. (6), at  $O(Fo^0)$ , is reduced to

$$\frac{\partial}{\partial X} \left( \tilde{k}(\theta_0) \frac{\partial \theta_0}{\partial X} \right) = 0 \quad (10)$$

subject to

$$\frac{\partial \theta_0}{\partial X} = 0, \quad \theta_0 = \theta_w(\tau) \quad \text{at } X=0 \quad (11)$$

At  $O(Fo^{-1})$ , we have

$$\tilde{c}_p(\theta_0) \frac{\partial \theta_0}{\partial \tau} = \frac{\partial}{\partial X} \left( \tilde{k}(\theta_0) \frac{\partial \theta_1}{\partial X} + \theta_1 \tilde{k}'(\theta_0) \frac{\partial \theta_0}{\partial X} \right) \quad (12)$$

subject to

$$\frac{\partial \theta_1}{\partial X} = 0, \quad \theta_1 = 0 \quad \text{at } X=0 \quad (13)$$

whilst at  $O(Fo^{-2})$ ,

$$\begin{aligned} \tilde{c}_p(\theta_0) \frac{\partial \theta_1}{\partial \tau} + \theta_1 \tilde{c}_p'(\theta_0) \frac{\partial \theta_0}{\partial \tau} &= \frac{\partial}{\partial X} \left( \tilde{k}(\theta_0) \frac{\partial \theta_2}{\partial X} + \theta_1 \tilde{k}'(\theta_0) \frac{\partial \theta_1}{\partial X} \right. \\ &\quad \left. + \left\{ \theta_2 \tilde{k}'(\theta_0) + \frac{1}{2} \theta_1^2 \tilde{k}''(\theta_0) \right\} \frac{\partial \theta_0}{\partial X} \right) \end{aligned} \quad (14)$$

subject to

$$\frac{\partial \theta_2}{\partial X} = 0, \quad \theta_2 = 0 \quad \text{at } X=0 \quad (15)$$

At  $O(Fo^{-3})$ ,

$$\begin{aligned} \tilde{c}_p(\theta_0) \frac{\partial \theta_2}{\partial \tau} + \theta_1 \tilde{c}_p'(\theta_0) \frac{\partial \theta_1}{\partial \tau} + \left\{ \theta_2 \tilde{c}_p'(\theta_0) + \frac{1}{2} \theta_1^2 \tilde{c}_p''(\theta_0) \right\} \frac{\partial \theta_0}{\partial \tau} \\ = \frac{\partial}{\partial X} \left( \tilde{k}(\theta_0) \frac{\partial \theta_3}{\partial X} + \tilde{k}'(\theta_0) \frac{\partial(\theta_1 \theta_2)}{\partial X} + \frac{1}{6} \tilde{k}''(\theta_0) \frac{\partial(\theta_1^3)}{\partial X} \right) \\ + \frac{\partial}{\partial X} \left( \left[ \tilde{k}'(\theta_0) \theta_3 + \tilde{k}''(\theta_0) \theta_1 \theta_2 + \frac{1}{6} \tilde{k}'''(\theta_0) \theta_1^3 \right] \frac{\partial \theta_0}{\partial X} \right) \end{aligned} \quad (16)$$

subject to

$$\frac{\partial \theta_3}{\partial X} = 0, \quad \theta_3 = 0 \quad \text{at } X=0 \quad (17)$$

Here, primes denote differentiation with respect to  $\theta$ .

From these, it becomes clear that we have obtained from the original inverse formulation a sequence of direct problems for the terms in the asymptotic expansion. In particular, we arrive at

$$\theta_0(X, \tau) = \theta_w(\tau) \quad (18)$$

$$\theta_1(X, \tau) = \frac{1}{2} \left( \frac{\tilde{c}_p(\theta_w)}{\tilde{k}(\theta_w)} \right) \dot{\theta}_w(\tau) X^2 \quad (19)$$

$$\theta_2(X, \tau) = \frac{\tilde{c}_p^2(\theta_w)}{24\tilde{k}^2(\theta_w)} \left( \dot{\theta}_w + 2 \left\{ \frac{\tilde{c}_p'(\theta_w)}{\tilde{c}_p(\theta_w)} - 2 \frac{\tilde{k}'(\theta_w)}{\tilde{k}(\theta_w)} \right\} \dot{\theta}_w^2 \right) X^4 \quad (20)$$

where dots denote differentiation with respect to  $\tau$ . These are essentially the solutions obtained by Burggraf [2], although for this paper we also evaluated  $\theta_3$  using the Maple symbolic manipulation package [4]. The subsequent expression is extremely lengthy, and we do not present it here. Using these, we can arrive at the appropriate asymptotic expansion for the heat transfer coefficient, which turns out to be of the form

$$h = \frac{[k]Fo^{-1}}{L} \{h_0 + Fo^{-1}h_1 + Fo^{-2}h_2 + O(Fo^{-3})\}$$

where

$$h_0 = -\frac{\tilde{c}_p(\theta_w) \dot{\theta}_w}{\theta_w - \theta_\infty} \quad (21)$$

$$\begin{aligned} h_1 = \frac{-\tilde{c}_p^2(\theta_w)}{6\tilde{k}(\theta_w)(\theta_w - \theta_\infty)} \left[ \dot{\theta}_w + \left( 2 \frac{\tilde{c}_p'(\theta_w)}{\tilde{c}_p(\theta_w)} - \frac{\tilde{k}'(\theta_w)}{\tilde{k}(\theta_w)} \right. \right. \\ \left. \left. - \frac{3}{(\theta_w - \theta_\infty)} \right) \dot{\theta}_w^2 \right] \end{aligned} \quad (22)$$

The expression for  $h_2$  is also lengthy and not presented here.

Issues that are of some interest here are whether the solution generated in this way is stable and whether the asymptotic series is convergent. As for stability, it is well-known (e.g., [8]) that the method is unstable, since arbitrarily small changes in  $\theta_w$  can lead to large errors in  $h$ . From a practical point of view, as our comparison of analytical and numerical results will show, the impact of this on the quality of the method or solution decreases as  $Fo$  increases. As for convergence, some guidelines can be obtained for the linear IHCP using the Stefan solution for  $\theta$ , which can be written as

$$\theta(X, \tau) = \sum_{i=0}^{\infty} Fo^{-i} \frac{d^i \theta_w}{d\tau^i}(\tau) \frac{X^{2i}}{(2i)!}. \quad (23)$$

This suggests that the solution should be convergent for all values of  $Fo$ , provided that  $\theta_w$  is infinitely differentiable. For the non-linear IHCP, however, there cannot be any corresponding statement, and the issue can only be resolved, in general numerically, on a case-by-case basis for different  $\theta_w$ .

### Asymptotic Analysis for $Fo \gg 1$ : Rings

We consider an analogous formulation for a quenched ring, assumed to be one-dimensional (no axial variation). Consider the cooling of a steel ring of thickness  $2L$ , initially at a uniform temperature  $T_i$ . At time  $t > 0$ , the outer and the inner surfaces of the ring, taken to be at  $\bar{r} = r_c \pm L$  respectively, are subjected to cooling characterized by a time-dependent heat transfer coefficient  $h(t)$ . One-dimensional heat conduction in the ring is then given by

$$\rho c_p(T) \frac{\partial T}{\partial t} = \frac{1}{\bar{r}} \frac{\partial}{\partial \bar{r}} \left( \bar{r} k(T) \frac{\partial T}{\partial \bar{r}} \right) \quad (24)$$

Again, we require that the maximum temperature should not exceed  $T_w(t)$ ; however, unlike the plate, it is not possible to specify *a priori* where in the ring this will be, since there is no available symmetry condition; furthermore, it is possible that the location of

this point with maximum temperature is a function of time. Taking the heat transfer coefficients on the inner and outer surfaces to be  $h_-(t)$  and  $h_+(t)$  respectively, we have

$$k \frac{\partial T}{\partial \bar{r}} = \mp h_{\pm}(t)(T - T_{\infty}) \quad \text{at } \bar{r} = r_c \pm L \quad (25)$$

Nondimensionalising for  $t$  and  $T$  as before, but now with  $R = \bar{r}/L$ , Eqs. (24) and (25) become, respectively,

$$\tilde{c}_p(\theta) \frac{\partial \theta}{\partial \tau} = \text{Fo} \frac{1}{R} \frac{\partial}{\partial R} \left( R \tilde{k}(\theta) \frac{\partial \theta}{\partial R} \right) \quad (26)$$

and

$$\left( \frac{[k]}{L} \right) \tilde{k}(\theta) \frac{\partial \theta}{\partial R} = \mp h_{\pm}(\tau)(\theta - \theta_{\infty}) \quad \text{at } R = R_c \pm 1 \quad (27)$$

where  $R_c = r_c/L$ .

The thin ring limit does, however, permit some analytical progress. Writing  $R_c = \varepsilon^{-1} (\ll 1)$ , and introducing

$$\tilde{R} = R - \frac{1}{\varepsilon}$$

we have for  $-1 \leq \tilde{R} \leq 1$ ,

$$\tilde{c}_p(\theta) \frac{\partial \theta}{\partial \tau} = \frac{\text{Fo}}{1 + \varepsilon \tilde{R}} \frac{\partial}{\partial \tilde{R}} \left( [1 + \varepsilon \tilde{R}] \tilde{k}(\theta) \frac{\partial \theta}{\partial \tilde{R}} \right) \quad (28)$$

and

$$\left( \frac{[k]}{L} \right) \tilde{k}(\theta) \frac{\partial \theta}{\partial \tilde{R}} = \mp h_{\pm}(\tau)(\theta - \theta_{\infty}) \quad \text{at } \tilde{R} = \pm 1 \quad (29)$$

This time, we have two small parameters,  $\text{Fo}^{-1}$  and  $\varepsilon$ , and the form of the asymptotic series will depend on their relative magnitudes. Typically (see physical parameters below),  $\text{Fo}^{-1} \sim \varepsilon$ , although this feature only turns out to affect the solution at  $O(\text{Fo}^{-2})$ , as shown below.

At  $O(\text{Fo}^0)$ , we have

$$\frac{\partial}{\partial \tilde{R}} \left( \tilde{k}(\theta_0) \frac{\partial \theta_0}{\partial \tilde{R}} \right) = 0 \quad (30)$$

subject to

$$\left( \frac{[k]}{L} \right) \tilde{k}(\theta_0) \frac{\partial \theta_0}{\partial \tilde{R}} = 0 \quad \text{at } \tilde{R} = \pm 1 \quad (31)$$

Equation (30) now requires that  $\tilde{k}(\theta_0) \partial \theta_0 / \partial \tilde{R}$  is a function of  $\tau$ , but Eq. (31) implies that the only possibility is  $\partial \theta_0 / \partial \tilde{R} = 0$ . This, combined with the requirement that the temperature should not exceed  $\theta_w(\tau)$ , gives as before

$$\theta_0(\tilde{R}, \tau) = \theta_w(\tau) \quad (32)$$

Next, at  $O(\text{Fo}^{-1})$ , we have

$$\tilde{c}_p(\theta_0) \frac{\partial \theta_0}{\partial \tau} = \frac{\partial}{\partial \tilde{R}} \left( \tilde{k}(\theta_0) \frac{\partial \theta_1}{\partial \tilde{R}} + \theta_1 \tilde{k}'(\theta_0) \frac{\partial \theta_0}{\partial \tilde{R}} \right) \quad (33)$$

subject to

$$\tilde{k}(\theta_0) \frac{\partial \theta_1}{\partial \tilde{R}} = \mp h_{0\pm}(\tau)(\theta_0 - \theta_{\infty}) \quad \text{at } \tilde{R} = \pm 1 \quad (34)$$

where  $h_{0\pm}$  is the first term in the asymptotic series for  $h_{\pm}$ , through

$$h_{\pm} = \frac{[k]\text{Fo}^{-1}}{L} \{h_{0\pm} + \text{Fo}^{-1}h_{1\pm} + O(\text{Fo}^{-2})\}$$

The general form for the solution for  $\theta_1$  will be

$$\theta_1(\tilde{R}, \tau) = \frac{1}{2} \left( \frac{\tilde{c}_p(\theta_w)}{\tilde{k}(\theta_w)} \right) \dot{\theta}_w(\tau) \tilde{R}^2 + A_1(\tau) \tilde{R} + B_1(\tau) \quad (35)$$

Equation (34) can be used to obtain

$$A_1(\tau) = \frac{(h_{0-}(\tau) - h_{0+}(\tau))(\theta_w - \theta_{\infty})}{2\tilde{k}(\theta_w)}$$

which implies that, regardless of the form of  $B_1(\tau)$ , the location of the maximum temperature is to be found at

$$\tilde{R} = - \frac{(h_{0-}(\tau) - h_{0+}(\tau))(\theta_w - \theta_{\infty})}{2\tilde{c}_p(\theta_w) \dot{\theta}_w}$$

Furthermore, this point will move outwards if  $h_{0-}(\tau) > h_{0+}(\tau)$ , inwards otherwise. Conversely, and analogous to Eq. (21), we have the result that the ring cools with the profile  $\theta_w(\tau)$  at leading order provided that

$$h_{0+}(\tau) + h_{0-}(\tau) = \frac{-2\tilde{c}_p(\theta_w) \dot{\theta}_w}{(\theta_w - \theta_{\infty})} \quad (36)$$

Also, to ensure that the temperature at the hottest point of the ring should not exceed  $\theta_w(\tau)$ , we require

$$B_1(\tau) = \frac{(h_{0-}(\tau) - h_{0+}(\tau))^2 (\theta_w - \theta_{\infty})^2}{8\tilde{k}(\theta_w) \tilde{c}_p(\theta_w) \dot{\theta}_w}$$

Note that in the case when  $h_{0-}(\tau) = h_{0+}(\tau)$ , the thin plate solution for  $\theta_1$  is recovered, as is the expression for  $h_0$  in Eq. (21).

At  $O(\text{Fo}^{-2})$ , setting  $\varepsilon = \chi \text{Fo}^{-1}$ , where  $\chi$  is an  $O(1)$  constant, we have

$$\begin{aligned} & \left( \tilde{c}_p(\theta_w) \left( \frac{\partial \theta_1}{\partial \tau} + \chi \tilde{R} \frac{\partial \theta_w}{\partial \tau} \right) + \theta_1 \tilde{c}_p'(\theta_w) \frac{\partial \theta_w}{\partial \tau} \right) \\ &= \frac{\partial}{\partial \tilde{R}} \left( \tilde{k}(\theta_w) \left[ \frac{\partial \theta_2}{\partial \tilde{R}} + \chi \tilde{R} \frac{\partial \theta_1}{\partial \tilde{R}} \right] + \theta_1 \tilde{k}'(\theta_w) \frac{\partial \theta_1}{\partial \tilde{R}} \right) \end{aligned} \quad (37)$$

subject to

$$\begin{aligned} & \tilde{k}(\theta_w) \left( \frac{\partial \theta_2}{\partial \tilde{R}} - \frac{\theta_1}{\theta_w - \theta_{\infty}} \frac{\partial \theta_1}{\partial \tilde{R}} \right) + \tilde{k}'(\theta_w) \theta_1 \frac{\partial \theta_1}{\partial \tilde{R}} \\ &= \mp h_{1\pm}(\theta_w - \theta_{\infty}) \quad \text{at } \tilde{R} = \pm 1 \end{aligned} \quad (38)$$

We omit the remaining details here, except to comment that an equation for  $h_{1-}(\tau)$  and  $h_{1+}(\tau)$  analogous to Eq. (36) can be expected. Instead, we derive a solution based on the assumption that  $h_-(\tau) = h_+(\tau)$ . At  $O(\text{Fo}^0)$  and  $O(\text{Fo}^{-1})$ , the solutions for  $\theta_0$  and  $\theta_1$ , respectively, are the same as for the plate, but from Eq. (37) we see that  $\theta_2$  will have an antisymmetric component due to ring curvature. Proceeding as before, we have

$$\begin{aligned} \theta_2(\tilde{R}, \tau) &= \frac{\tilde{c}_p^2(\theta_w)}{24\tilde{k}^2(\theta_w)} \left( \dot{\theta}_w + 2 \left\{ \frac{\tilde{c}_p'(\theta_w)}{\tilde{c}_p(\theta_w)} - 2 \frac{\tilde{k}'(\theta_w)}{\tilde{k}(\theta_w)} \right\} \dot{\theta}_w^2 \right) \tilde{R}^4 \\ &\quad - \frac{\chi \tilde{c}_p(\theta_w) \dot{\theta}_w}{6\tilde{k}(\theta_w)} \tilde{R}^3 + A_2(\tau) \tilde{R} + B_2(\tau) \end{aligned} \quad (39)$$

From Eq. (38), we have

$$A_2(\tau) = \frac{\chi \tilde{c}_p(\theta_w) \dot{\theta}_w}{2\tilde{k}(\theta_w)} \quad (40)$$

with  $B_2(\tau)$  being chosen to ensure that  $\theta_2(\tilde{R}, \tau)$  is everywhere negative. Finally, we arrive at

$$h_1 = \frac{-\tilde{c}_p^2(\theta_w)}{6\tilde{k}(\theta_w)(\theta_w - \theta_\infty)} \left[ \tilde{\theta}_w + \left( 2 \frac{\tilde{c}_p'(\theta_w)}{\tilde{c}_p(\theta_w)} - \frac{\tilde{k}'(\theta_w)}{\tilde{k}(\theta_w)} - \frac{3}{(\theta_w - \theta_\infty)} \right) \tilde{\theta}_w^2 \right] \quad (41)$$

indicating that although the temperature is affected by the curvature at this order, the heat transfer coefficient is not.

## Numerical Solution

In what follows, the analytical solutions presented above are used to test our numerical scheme for the solution of the inverse problem. Furthermore, the availability of both analytical and numerical methods provides an estimate of the range of validity of the asymptotic series.

Numerous algorithms can be found in the literature for the nonlinear IHCP. Amongst these are the function specification method [9], space-marching techniques [6] and those based on the infinite dimensional adjoint method [7]. Here, we develop a variant on existing methods, in that we implement the function specification method [9] by means of the Keller Box scheme [10] and Newton iteration, a combination which, in spite of its versatility for the solution of nonlinear parabolic direct problems, appears not to have been used at all for inverse problems of this type. In fact, the method proves to be particularly suitable for handling the resulting sensitivity equations, as well as for updating the latest surface heat flux iterate, as shown below. In addition, it is not necessary to employ quasi-linearization of the temperature-dependent properties, as has been done in some numerical schemes [5,11,12]; this feature is desirable, since it ensures that the scheme remains second-order accurate in both time and space variables, which becomes of increasing importance if the thermal properties vary strongly with temperature. Thus, our treatment of the direct problem is accurate as it can be without going to higher-order schemes, and accuracy is only limited by the nature of the inverse algorithm, which is known to be unstable if too small time steps are used [9]; for details regarding numerical uncertainty, therefore, we refer to [9]. In what follows, we consider plate solutions, where the location of the maximum temperature is known; solutions for rings are postponed for future work.

Writing Eq. (6) as the two first-order equations

$$Q = \frac{\partial \theta}{\partial X} \quad (42)$$

$$\tilde{c}_p(\theta) \frac{\partial \theta}{\partial \tau} = \text{Fo} \frac{\partial}{\partial X} (\tilde{k}(\theta) Q) \quad (43)$$

and introducing a rectangular mesh with grid points at  $(\tau_j)_{j=0, \dots, M}$  and  $(X_i)_{i=0, \dots, N}$ , where  $M$  and  $N$  are the number of points in  $\tau$  and  $X$  respectively, the function specification method proceeds as follows. Assuming that  $\theta$  and  $Q$  have been determined for  $0 \leq \tau \leq \tau_{m-1}$ , where  $1 \leq m \leq M$ , we temporarily assume that  $Q_{N,k} = \beta$  for  $r$  future time steps ( $\tau_{m-1} \leq \tau \leq \tau_{m-1+r}$ ), and solve the direct problem for  $\tau = \tau_m, \dots, \tau_{m-1+r}$ , with the boundary conditions  $Q_{N,k} = \beta$  and  $Q_{0,k} = \beta$  ( $k = m, \dots, m-1+r$ ). Next it is required to minimize the functional

$$S := \sum_{l=1}^r (\theta_{0,m-1+l} - \theta_w(\tau_{m-1+l}))^2 \quad (44)$$

with respect to  $\beta$ ; this requires  $\partial S / \partial \beta = 0$ , i.e.,

$$\sum_{l=1}^r (\theta_{0,m-1+l} - \theta_w(\tau_{m-1+l})) \frac{\partial \theta_{0,m-1+l}}{\partial \beta} = 0$$

which in turn requires knowledge about the sensitivity coefficients, i.e., the function  $\partial \theta / \partial \beta$ .

Defining  $\tilde{\theta} := \partial \theta / \partial \beta$  and  $\tilde{Q} := \partial Q / \partial \beta$ , we obtain the governing equation for  $\tilde{\theta}$  by differentiating Eqs. (42) and (43) with respect to  $\beta$  to obtain

$$\tilde{Q} = \frac{\partial \tilde{\theta}}{\partial X} \quad (45)$$

$$\left( \tilde{c}_p(\theta) \frac{\partial \tilde{\theta}}{\partial \tau} + \tilde{c}_p'(\theta) \tilde{\theta} \frac{\partial \theta}{\partial \tau} \right) = \text{Fo} \frac{\partial}{\partial X} (\tilde{k}(\theta) \tilde{Q} + \tilde{k}'(\theta) \tilde{\theta} Q) \quad (46)$$

This is subject to the boundary conditions

$$\left. \begin{array}{l} \tilde{Q} = 0 \quad \text{at } X = 0 \\ \tilde{Q} = 1 \quad \text{at } X = 1 \end{array} \right\} \text{for } \tau_m \leq \tau \leq \tau_{m-1+r} \quad (47)$$

and the initial condition

$$\tilde{\theta} = 0 \quad \text{at } \tau = \tau_{m-1} \quad (48)$$

This constitutes a linear direct problem for  $\tilde{\theta}$  and  $\tilde{Q}$  which needs to be solved at every time step; this is in contrast to the linear IHCP for which the sensitivity coefficients can be determined once and for all with just one *a priori* computation.

Now writing

$$\varphi := \sum_{l=1}^r (\theta_{0,m-1+l} - \theta_w(\tau_{m-1+l})) \tilde{\theta}_{0,m-1+l} \quad (49)$$

we require  $\varphi = 0$ , for which an iterative loop for  $\beta$  is required. Denoting by  $v$  the iteration index for  $\beta$ , we update  $\beta$  using Newton iteration according to

$$\beta^{(v+1)} = \beta^{(v)} - \varphi \Big/ \frac{\partial \varphi}{\partial \beta}$$

where

$$\frac{\partial \varphi}{\partial \beta} = \sum_{l=1}^r (\theta_{0,m-1+l} - \theta_w(\tau_{m-1+l})) \frac{\partial \tilde{\theta}_{0,m-1+l}}{\partial \beta} + \sum_{l=1}^r \tilde{\theta}_{0,m-1+l}^2$$

For the linear IHCP, the sensitivity coefficients are independent of  $\beta$ , so that  $\partial \varphi / \partial \beta$  would already be available, since  $\tilde{\theta}$  has already been solved for. For the nonlinear IHCP, this is not the case, and additional variational equations for

$$\hat{\theta} := \frac{\partial \tilde{\theta}}{\partial \beta}, \quad \hat{Q} := \frac{\partial \tilde{Q}}{\partial \beta}$$

have to be solved. Differentiating Eqs. (45)–(48) with respect to  $\beta$  gives

$$\hat{Q} = \frac{\partial \hat{\theta}}{\partial X} \quad (50)$$

$$\left( \tilde{c}_p(\theta) \frac{\partial \hat{\theta}}{\partial \tau} + \tilde{c}_p'(\theta) \hat{\theta} \frac{\partial \theta}{\partial \tau} \right) = \text{Fo} \frac{\partial}{\partial X} (\tilde{k}(\theta) \hat{Q} + \tilde{k}'(\theta) \hat{\theta} Q) + q \quad (51)$$

where

$$q = \text{Fo} \frac{\partial}{\partial X} (2\tilde{k}'(\theta) \tilde{\theta} \tilde{Q} + \tilde{k}''(\theta) \tilde{\theta}^2 Q) - 2\tilde{c}_p'(\theta) \tilde{\theta} \frac{\partial \tilde{\theta}}{\partial \tau} - \tilde{c}_p''(\theta) \tilde{\theta}^2 \frac{\partial \theta}{\partial \tau}$$

subject to the boundary conditions

$$\left. \begin{array}{l} \hat{Q} = 0 \quad \text{at } X = 0 \\ \hat{Q} = 0 \quad \text{at } X = 1 \end{array} \right\} \text{for } \tau_m \leq \tau \leq \tau_{m-1+r} \quad (52)$$

and the initial condition

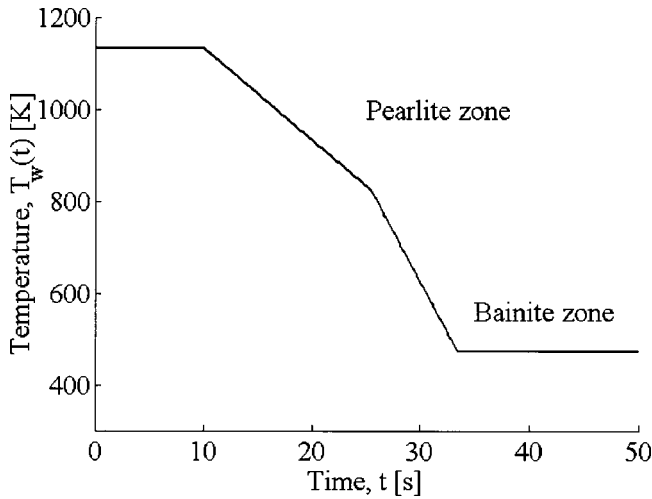


Fig. 3 Cooling curve used in this study

$$\hat{\theta} = 0 \text{ at } \tau = \tau_{m-1} \quad (53)$$

This also constitutes a linear direct problem for  $\hat{\theta}$  and  $\hat{Q}$  which needs to be solved at every time step.

Finally in this section, we note the computational budget for this method in order to advance one time step, relative to the budget for a one-step advance for the nonlinear direct problem. With the convergence criterion at the  $j$ th time step for Eqs. (42) and (43) taken to be

$$\max_{i=0, \dots, N} (|\theta_{i,j}^{(n+1)} - \theta_{i,j}^{(n)}|, |Q_{i,j}^{(n+1)} - Q_{i,j}^{(n)}|) < 10^{-9}$$

the number of Newton iterations  $N_{\text{newt}}$  was typically found to be 3–4. However, a one time-step advance for the nonlinear inverse problem requires

- 1) Eqs. (42) and (43) to be solved over  $r$  time steps ( $rN_{\text{newt}}$  operations);
- 2) Eqs. (45) and (46) to be solved over  $r$  time steps ( $r$  operations);
- 3) Eqs. (50) and (51) to be solved over  $r$  time steps ( $r$  operations);
- 4) steps 1–3 to be repeated until convergence for  $\beta$  is obtained ( $rN_{\text{var}}(N_{\text{newt}} + 2)$  operations).

Here, one “operation” is denoted to mean the solution of  $(M + 1)$  linear equations, either those arising from the linearisation in step 1, or those in steps 2 and 3. In summary, the total budget ratio is found to be

$$\frac{rN_{\text{var}}(N_{\text{newt}} + 2)}{N_{\text{newt}}}$$

so that, with  $N_{\text{var}}$  also typically 3–4, approximately  $6r$  as many operations are required to solve the inverse problem as are required to solve the direct problem. For the majority of computations carried out here, we took  $M = 201$ ,  $N = 100$ , and  $r = 4$ ; with these specifications, a solution was obtained within several seconds on a 500 MHz Compaq Alphaserber with 3GB RAM. Additional computations for  $N = 200$  were also carried out to test for grid independence in respect of the space variable,  $X$ ; no difference was observed between results for  $N = 100$  and  $N = 200$ , and subsequently only the coarser mesh was used. Of considerably greater significance is the total future time  $r\Delta\tau$ , where  $\Delta\tau$  is the mesh spacing in time; here, a uniform mesh was used throughout, so that  $\Delta\tau = 1/(M - 1)$ . The results of investigations of this combined effect are given in the next section. Additionally, since the numerical scheme is second-order accurate, we have that the nu-

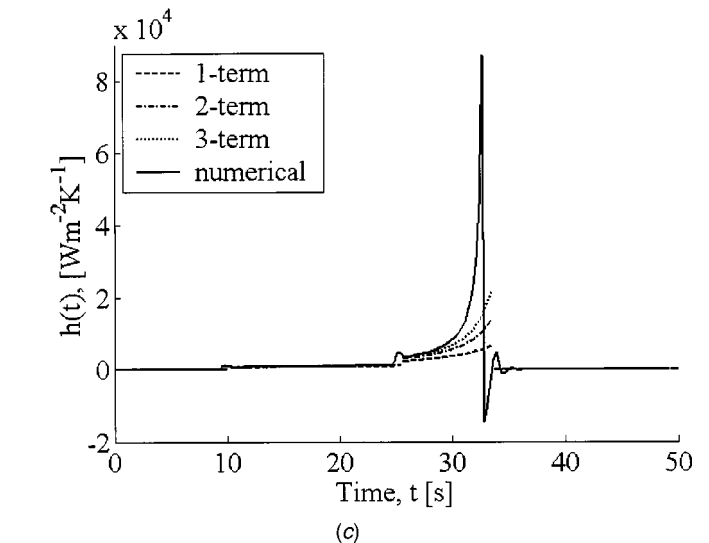
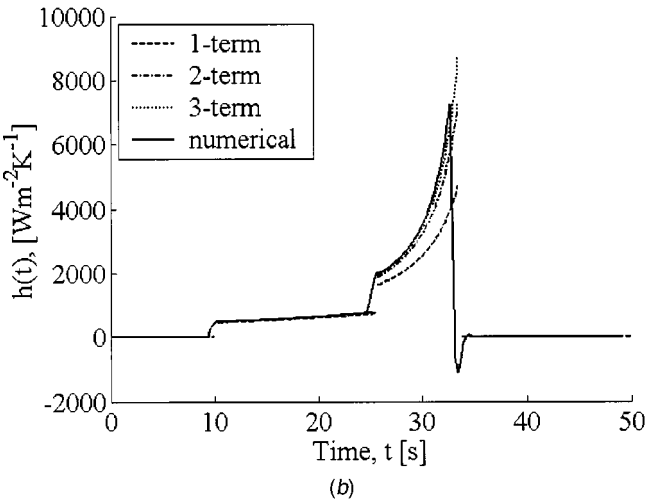
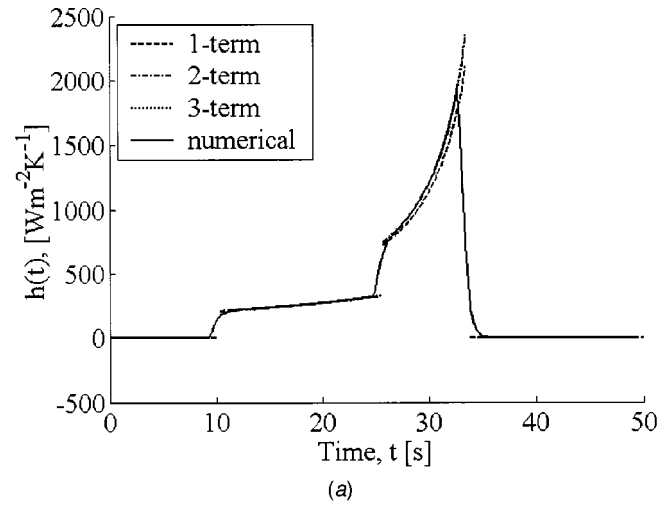
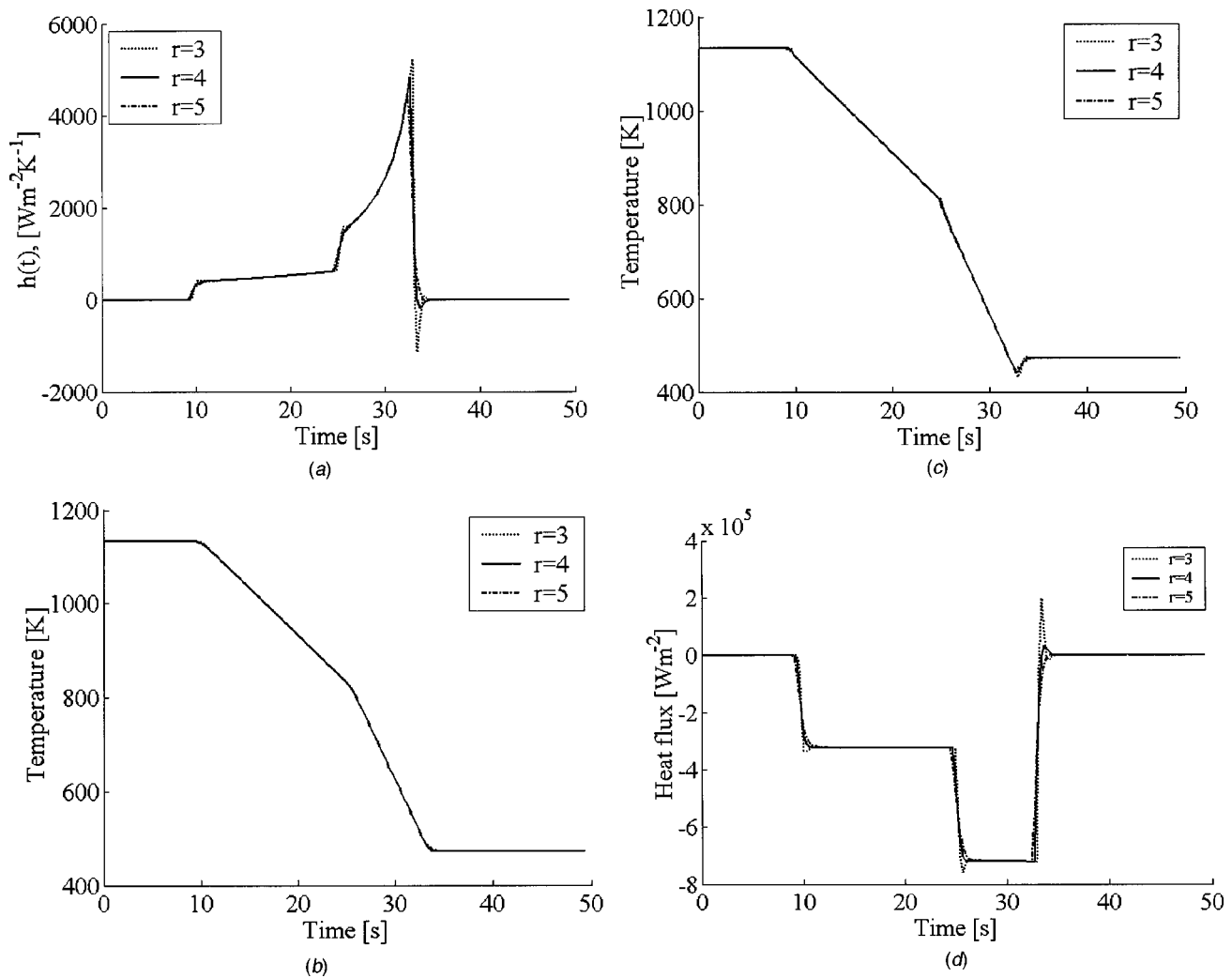


Fig. 4 The required convective heat transfer coefficient,  $h(t)$ , as calculated by the analytical method using 1, 2, and 3 series expansion terms, and by a numerical method: (a)  $\text{Fo}^{-1} = 0.02$ ; (b)  $\text{Fo}^{-1} = 0.1$ ; and (c)  $\text{Fo}^{-1} = 0.2$ .

merical uncertainty for all the runs is  $O(10^{-4})$ .

As for numerical validation of the scheme, this is provided in the next section through comparison with truncations of the asymptotic series. In addition, the code was checked against the



**Fig. 5 Selected quantities as numerically computed for 3, 4, and 5 future time steps in the model ( $Fo^{-1}=0.07$ ): (a) the convective heat transfer coefficient,  $h(t)$ , at  $x=L$ ; (b) the temperature,  $T_w(t)$ , at  $x=0$ ; (c) the surface temperature at  $x=L$ ; and (d) the surface heat flux at  $x=L$ .**

test case of a triangular heat flux given in [9] (e.g., see p. 169), and excellent agreement was found, although for the sake of brevity we do not present the results here.

## Results

The analytical and numerical considerations given above are implemented for the quenching of SAE 52100 steel. The physical properties used are:

$$k(T)=k_0+k_1T, \quad c_p(T)=c_0 \quad (54)$$

so that  $[k]=k_0$ ,  $[c_p]=c_0$ , and then

$$\tilde{k}(\theta)=1+\mu\theta, \quad \tilde{c}_p(\theta)=1$$

where  $\mu=k_1T_i/k_0$ . We take  $T_i=860$  C,  $T_f=20$  C,  $t_f=50$  s,  $c_0=635$  Jkg $^{-1}$  C $^{-1}$ ,  $k_0=15.0$  Wm $^{-1}$  C $^{-1}$ ,  $k_1=0.0142$  Wm $^{-1}$  C $^{-2}$ ,  $\rho=7810$  kgm $^{-3}$ . As for geometrical parameters, the computations are based around the quenching of a ring with inner radius 0.028 m and outer radius 0.034 m. Consequently, we have  $L=0.003$  m and  $r_c=0.031$  m, and so  $Fo^{-1}\approx 0.07$ ,  $\varepsilon\approx 0.1$ . Thus, although we present only solutions for a plate, they should constitute good first approximations to a ring of the same thickness.

Results are presented for the cooling curve shown in Fig. 3, which has been constructed in such a way that it approaches the 1 percent pearlite “nose” more closely than would a conventional

constant cooling curve and thus allow slowest cooling rates (which is industrially desirable both to minimize cooling cost and product distortion); after that, more rapid cooling is used to avoid the 1 percent bainite “nose.” Using Eqs. (21) and (22), we have

$$h_0=\frac{-\dot{\theta}}{\theta_w-\theta_\infty}$$

$$h_1=\frac{-1}{6(1+\mu\theta_w)(\theta_w-\theta_\infty)}\left[\ddot{\theta}_w-\frac{\mu\dot{\theta}_w^2}{(1+\mu\theta_w)}-\frac{3\dot{\theta}_w^2}{(\theta_w-\theta_\infty)}\right]$$

It is instructive to discuss the behavior of the solution in terms of the value of  $Fo^{-1}$ . This is done in Figs. 4(a–c), which compare the heat transfer coefficients for the asymptotic analytical solution and the numerical solution for  $Fo^{-1}=0.02, 0.1$ , and  $0.2$ , respectively.

In Fig. 4(a), good agreement is obtained between the results of the numerical method and the one and two-term expansions of the analytical method. At gradient discontinuities of  $T_w(t)$ , the analytical method gives discontinuities in  $h(t)$ , whereas the numerical scheme smoothes these out. Note here the interpretations of the solution behavior at each of these three discontinuities. For the first two, the behavior is similar, with a moderately rapid increase in the heat transfer coefficient being necessary to attain the desired temperature profile; at the third, however, an initially

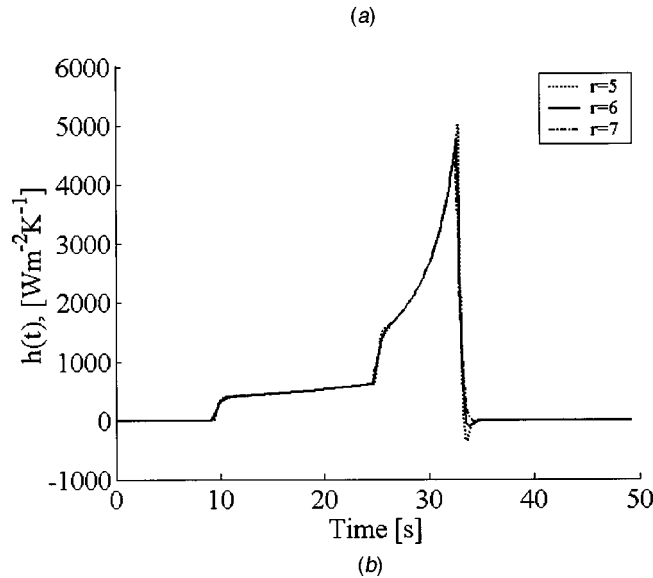
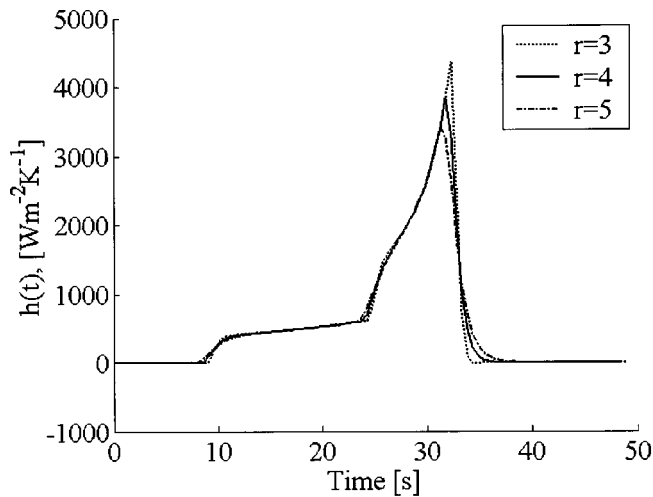


**Fig. 6** The convective heat transfer coefficient,  $h(t)$ , at  $x=L$  for  $Fo^{-1}=0.07$  with: (a)  $\Delta\tau=1/100$ ,  $r=3, 4, 5$ ; and (b)  $\Delta\tau=1/300$ ,  $r=5, 6, 7$ .

negative value, corresponding to heating, is required. Note also that the peak prior to this discontinuity is not due to the discontinuity itself, but simply as a consequence of the fact that  $\theta_w$  is decreasing whilst  $\dot{\theta}_w$  is constant (cf. Eq. (21)).

Increasing  $Fo^{-1}$  further to  $Fo^{-1}=0.1$ , Fig. 4(b) shows that, for the final part of the quenching curve, an oscillation in  $h(t)$  appears in order to maintain the desired temperature of  $200^\circ\text{C}$ ; this we interpret as an instability in our numerical scheme which arises as  $Fo^{-1}$  is increased, in combination with the sudden jump in the gradient of  $T_w(t)$ . Prior to this, we see that the three truncated asymptotic series agree well with the numerical solution until 25 s, but then the one-term series severely underpredicts the required heat transfer coefficient; the two-term series performs significantly better, and the three-term series better still, but it appears that more terms in the asymptotic expansion would be necessary to provide even better agreement.

In Fig. 4(c) for  $Fo^{-1}=0.2$ , it becomes even clearer that further terms in the asymptotic expansion must be added, although as in Fig. 4(b) the trend appears to be in the right direction. An important mathematical point here is that since the asymptotic solution is composed of analytical solutions to ordinary differential equations, it is free of the oscillations that a numerical solution to a partial differential equations may possess due, for example, to

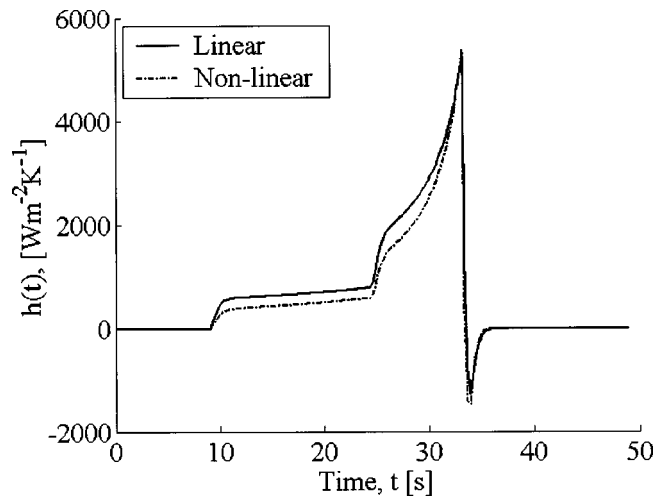


**Fig. 7** Comparison of the numerically computed convective heat transfer coefficient with constant (“linear”) and temperature-dependent (“nonlinear”) thermal conductivity ( $Fo^{-1}=0.07, r=4$ )

unsmooth boundary conditions; as a consequence, the asymptotic series may provide a useful, and often very accurate, approximation to the full numerical solution, provided enough terms are calculated. For this case, the numerical instability mentioned in Fig. 4(b) appears to be even more severe for  $r=4$ , with oscillations occurring at all three gradient discontinuities of  $T_w(t)$ . However, as shown below, the way to alleviate these appears to be to increase the value of  $r$ .

We give also some results for a plate for which  $Fo^{-1}=0.07$ . Fig. 5(a) demonstrates the effect of the number of future time steps used,  $r$ , on the heat transfer coefficient; the effect appears to be noticeable only at the gradient discontinuities of  $T_w(t)$ , but we notice here that increasing  $r$  from 3 to 5 removes the unphysical oscillation at  $t=33$  s. Figure 5(b) gives a comparison of the specified temperature  $T_w(t)$ , with that actually computed numerically for  $r=3,4,5$ . Note here that whilst the numerical scheme copes well with the first two gradient discontinuities, it copes less well with the third, with the functional  $S$  in Eq. (44) being minimized in such a way that the computed temperature undershoots the desired profile (cf. Fig. 3), although the extent of the undershoot decreases with increased  $r$ . Fig. 5(c) gives the temperature profile at the quenched surface, and a comparison of Figs. 5(b) and 5(c) indicates the extent to which plate is a lumped body. Fig. 5(d) shows the heat flux at the quenched surface; here, as in Fig. 5(a), the higher values of  $r$  appear to confer increased stability on the solution at the gradient discontinuities of  $T_w(t)$ .

Figures 6(a) and 6(b), in tandem with Fig. 5(a), explore the combined effect of  $r\Delta\tau$  on the solution for  $Fo^{-1}=0.07$ . As is evident, all perform in qualitatively similar fashion, but perhaps the most interesting quantitative conclusion concerns the stability of the scheme near  $t=33$  s. In particular, the common feature we find is that the non-physical oscillations in  $h(t)$  there can be removed provided that  $r\Delta\tau$  exceeds a certain critical value: in Fig. 5(a), this value is in the range  $[0.02, 0.025]$ ; for Fig. 6(a),  $[0.033, 0.04]$ ; for Fig. 6(b)  $[0.02, 0.0233]$ .

Finally, Fig. 7 compares the results of a nonlinear computation, using Eq. (54), with those of a linear one where the thermal conductivity is taken to be

$$k(T) \equiv k_0 + k_1 T_{av}$$

where  $T_{av} = 530^\circ\text{C}$ , the average of the start and end temperatures. As is apparent, for this particular case, the linear formulation leads to an underestimate in the heat transfer coefficient required to obtain the desired quenching conditions.

## Conclusions

This paper has considered a one-dimensional nonlinear inverse heat conduction problem in the industrial process of quenching, using both analytical and numerical methods. The governing equations were nondimensionalised and the Fourier number (Fo) was identified as a key controlling dimensionless parameter. Asymptotic series could be constructed using this parameter, and these were found on the whole to compare well with results from a numerical scheme that was also implemented. The nature of the cooling temperature profile used, a piecewise linear function of time, indicates some of the features of inverse problems with unsmooth boundary conditions: whilst both methods agree well on smooth portions of the cooling profile, difficulties were encountered with the numerical scheme at gradient discontinuities, although not necessarily so. Associated with this is the number of future time steps,  $r$ , that were required. Where the cooling curve is smooth,  $r=3$  was sufficient; otherwise, as many as 5 or 6 were necessary to stabilize the solution after a gradient discontinuity, and our experiences show that higher values of  $\text{Fo}^{-1}$ , corresponding to thicker geometries, lead to greater difficulties in this respect. As for the asymptotic series, it proved advisable to use a symbolic manipulator to compute its terms, since the algebra becomes exceedingly lengthy after just a couple of terms. However, a two-term series appeared to be sufficient for predicting the heat transfer coefficient to within a couple of percent for Fo as high as 10 for the cooling curves used here.

This work is our first attempt to couple heat transfer to the control of phase transformations in quenching in an inverse way, i.e., by predicting the convective heat transfer coefficient that would be necessary to produce a quenched product with a desired composition, and which follows the progress of the phase transformation in a way which tends to optimize the process (see, for instance, [13] for another example, although not related to quenching). The plate/ring quenching analogy provided here was useful for sufficiently large values of the Fourier number, although solutions were presented mainly for the plate. Finally, we should note the advantages of the twin analytical/numerical approach presented here. In particular, nondimensionalisation identifies the magnitudes of key controlling parameters, and thence possibly simple closed-form series solutions that would not have been evident from the original formulation. These solutions can then serve as a quantitative check against numerical algorithms for the IHCP; in fact, to the authors' knowledge, this may well be the first time that this has been done. In particular, we note how the approaches complement each other as  $\text{Fo}^{-1}$  is increased (cf. Figs. 4(a-c)): the numerical approach gives the desired solution, although this can prove unreliable as a singularity in the boundary conditions is reached; at this point, the analytical solution can provide a guide as to how the desired solution should behave. In addition, the fact that we have implemented the versatile and efficient Keller Box scheme within an inverse problem setting indicates that it should be possible to incorporate, in an expedient way, more of the physical features associated with gas quenching, such as phase transformations and distortion.

Naturally, a full treatment of a coupled inverse/optimization problem of this sort in gas quenching would involve the inverse prediction of the optimal time-dependent heat transfer coefficients in three dimensions for arbitrary complex geometries, with all physical phenomena modeled in the numerical simulation. Nevertheless, the validation of computer codes for such calculations would require benchmark comparisons in simple geometries, such as those presented here. Finally, the algorithm presented would be useful in practice in reducing computational time for inverse problems involving simpler geometries, where there is no need to use the full multidimensional functionality typically provided in vendor software.

## Acknowledgment

This work was partially supported by AGA AB, SKF Engineering and Research Center, B.V., Volvo Personvagnar Komponenter AB and Ipsen International GmbH.

## Nomenclature

- $c_p(T)$  = temperature-dependent specific heat capacity,  $\text{Jkg}^{-1}\text{K}^{-1}$
- $\bar{c}_p(\theta)$  = dimensionless temperature-dependent dimensionless specific heat capacity
- $[c_p]$  = specific heat capacity scale,  $\text{Jkg}^{-1}\text{K}^{-1}$
- $\text{Fo}$  = Fourier number
- $h(t)$  = time-dependent heat transfer coefficient,  $\text{Wm}^{-2}\text{K}^{-1}$
- $(h_i)_{i=0,1,\dots}$  = terms in the asymptotic expansion for  $h(t)$
- $h_{\pm}(t)$  = time-dependent heat transfer coefficient on inner and outer ring surfaces,  $\text{Wm}^{-2}\text{K}^{-1}$
- $(h_{i\pm})_{i=0,1,\dots}$  = terms in the asymptotic expansion for  $h_{\pm}(t)$
- $k(T)$  = temperature-dependent thermal conductivity,  $\text{Wm}^{-1}\text{K}^{-1}$
- $\bar{k}(\theta)$  = dimensionless temperature-dependent dimensionless thermal conductivity
- $[k]$  = thermal conductivity scale,  $\text{Wm}^{-1}\text{K}^{-1}$
- $L$  = plate/ring half thickness, m
- $M$  = number of points for discretisation in  $\tau$
- $N$  = number of points for discretisation in  $X$
- $N_{\text{newt}}$  = number of Newton iterations for Eqs. (42) and (43)
- $N_{\text{var}}$  = number of times that the variational equations (50) and (51) are solved
- $q$  = source term in Eq. (51)
- $Q$  =  $\partial\theta/\partial X$
- $\bar{Q}$  =  $\partial Q/\partial\beta$
- $\hat{Q}$  =  $\partial\bar{Q}/\partial\beta$
- $\bar{r}$  = radial coordinate (ring), m
- $R$  = dimensionless radial coordinate (ring)
- $\bar{R}$  = scaled dimensionless radial coordinate (ring)
- $r_c$  = average ring radius, m
- $R_c$  = dimensionless average ring radius
- $r$  = number of future time steps used for the function specification method
- $S$  = functional defined in Eq. (44)
- $t$  = time, s
- $T$  = temperature, K
- $t_f$  = quenching end time, seconds
- $T_i$  = initial uniform temperature, K
- $T_w(t)$  = time-dependent desired quenching temperature, K
- $T_{\infty}$  = ambient temperature, K
- $x$  = normal coordinate (plate), m
- $X$  = dimensionless normal coordinate (plate)
- $\beta$  = guess for  $\partial\theta/\partial X$  at quenched surface
- $\varepsilon$  = reciprocal of the dimensionless average ring radius ( $R_c^{-1}$ )
- $\theta$  = dimensionless temperature
- $\bar{\theta}$  =  $\partial\theta/\partial\beta$
- $\hat{\theta}$  =  $\partial\bar{\theta}/\partial\beta$
- $\theta_w(\tau)$  = dimensionless desired quenching temperature
- $(\theta_i)_{i=0,1,\dots}$  = terms in the asymptotic expansion for  $\theta$
- $\theta_{\infty}$  = dimensionless ambient temperature
- $\rho$  = density,  $\text{kgm}^{-3}$
- $\tau$  = dimensionless time
- $\varphi$  = functional defined in Eq. (49)
- $\chi$  =  $O(1)$  constant ( $\varepsilon\text{Fo}$ )

## References

- [1] Thuvander, A., Melander, A., Lind, M., Lior, N., and Bark, F., 1999, "Prediction of Convective Heat Transfer Coefficients and Their Effects on Distortion

- and Mechanical Properties of Cylindrical Steel Bodies Quenched by Gas Cooling," Paper AJTE99-6289, presented at ASME/JSME Joint Thermal Engng. Conf., San Diego, CA, March 15–19, 1999.
- [2] Burggraf, O. R., 1964, "An Exact Solution of the Inverse Problem in Heat Conduction Theory and Applications," *ASME J. Heat Transfer*, **86C**, pp. 373–382.
- [3] Özişik, M. N., and Orlande, H. R. B., 2000, *Inverse Heat Transfer*, Taylor & Francis, New York.
- [4] <http://www.maplesoft.com>
- [5] Beck, J. V., Litkouhi, B., and St. Clair, C. R., Jr., 1982, "Efficient Sequential Solution of the Nonlinear Inverse Heat Conduction Problem," *Numer. Heat Transfer*, **5**, pp. 275–286.
- [6] Raynaud, M., and Bransier, J., 1986, "A New Finite-Difference Method for the Nonlinear Inverse Heat Conduction Problem," *Numer. Heat Transfer*, **9**, pp. 27–42.
- [7] Jarny, Y., Özişik, M. N., and Bardon, J. P., 1991, "A General Optimization Method Using Adjoint Equation for Solving Multidimensional Inverse Heat Conduction," *Int. J. Heat Mass Transf.*, **34**, pp. 2911–2919.
- [8] Alifanov, O. M., 1994, *Inverse Heat Transfer Problems*, Springer-Verlag.
- [9] Beck, J. V., Blackwell, B., and St. Clair, C. R., Jr., 1985, *Inverse Heat Conduction-III Posed Problems*, Wiley, New York.
- [10] Cebeci, T., and Bradshaw, P., 1984, *Physical and Computational Aspects of Convective Heat Transfer*, Springer, Berlin.
- [11] Archambault, P., and Azim, A., 1995, "Inverse Resolution of the Heat-Transfer Equation: Application to Steel and Aluminum Alloy Quenching," *J. Mater. Eng. Perform.*, **4**, pp. 730–736.
- [12] Archambault, P., Denis, S., and Azim, A., 1997, "Inverse Resolution of the Heat-Transfer Equation With Internal Heat Source: Application to the Quenching of Steels With Phase Transformations," *J. Mater. Eng. Perform.*, **6**, pp. 240–246.
- [13] Matsevityi, Y. M., Multanovskii, A. V., and Nemirovskii, I. A., 1991, "Optimization of the Heat-Engineering Processes Involving Utilization of Control and Identification Methods," *J. Eng. Phys.*, **59**, pp. 1055–1063.